Hindawi Publishing Corporation
Shock and Vibration
Volume 2014, Article ID 738162, 9 pages
http://dx.doi.org/10.1155/2014/738162

Research Article

The Analysis of Curved Beam Using B-Spline Wavelet on Interval Finite Element Method

Zhibo Yang,[1,2] Xuefeng Chen,[1,2] Yumin He,[3] Zhengjia He,[1,2] and Jie Zhang[1,2]

[1] *The State Key Laboratory for Manufacturing Systems Engineering, Xi'an 710049, China*
[2] *School of Mechanical Engineering, Xi'an Jiaotong University, Xi'an 710049, China*
[3] *College of Mechanical and Electrical Engineering, Xi'an University of Architecture and Technology, Xi'an 710049, China*

Correspondence should be addressed to Zhibo Yang; yangbo-5-7@163.com and Xuefeng Chen; chenxf@mail.xjtu.edu.cn

Received 30 January 2013; Accepted 26 October 2013; Published 25 February 2014

Academic Editor: Reza Jazar

A B-spline wavelet on interval (BSWI) finite element is developed for curved beams, and the static and free vibration behaviors of curved beam (arch) are investigated in this paper. Instead of the traditional polynomial interpolation, scaling functions at a certain scale have been adopted to form the shape functions and construct wavelet-based elements. Different from the process of the direct wavelet addition in the other wavelet numerical methods, the element displacement field represented by the coefficients of wavelets expansions is transformed from wavelet space to physical space by aid of the corresponding transformation matrix. Furthermore, compared with the commonly used Daubechies wavelet, BSWI has explicit expressions and excellent approximation properties, which guarantee satisfactory results. Numerical examples are performed to demonstrate the accuracy and efficiency with respect to previously published formulations for curved beams.

1. Introduction

Curved beams, which are also called arches in some fields, are well established due to their capacity of transferring loads through the combined action of bending and stretching. They are more efficient than straight beams. However, compared with the analysis of straight beams, the analysis of curved beams is more complex due to the presence of bending stretching coupling. Besides, the effects of shear deformation and rotatory inertia also increase the complexity. Static analysis neglecting these effects can lead to inaccuracies especially when the ratio of length to thickness is small. It is the same with the free vibration analysis, which results in erroneous frequencies and mode shapes for higher modes [1]. Thus, it is difficult to solve this problem exactly due to the aforementioned reasons. Although the energy methods such as Castigliano's theorem can be used to obtain the deflections, they are only useful in solving some simple problems [2]. The Rayleigh-Ritz is also an alternative method for the analysis of arches. However, its accuracy depends on the selection of displacement function and the chosen displacement function must satisfy the boundary condition, which turns out to restrict the application of the Rayleigh-Ritz method seriously. As an improvement of the Rayleigh-Ritz method, the finite element method (FEM) is widely used now in solving complex boundary problems.

In the finite element analysis of curved structures, the use of curved beam element is an efficient alternative to the use of large number of straight beam element to approximate the geometric shape of arches. However, many kinds of successful shape functions used in straight beam result in slow convergence or poor performance when they are applied to arches [3]. In the early studies [4, 5], there was a main view that it is the ignorance of the explicit rigid body motion that results in the slow convergence and poor performance of elements. Meck [6] showed that the unsatisfactory performance of curved elements is not due to the neglect of rigid body motions but due to the neglect of coupling required between normal and tangential displacements to satisfy the condition of inextensibility. Then he suggested the use of an independent interpolation for normal and tangential displacements to get a good result. Yamamoto and Ohtsubo [7] verified that cubic and quartic are the suitable orders of shape functions for curved beam element.

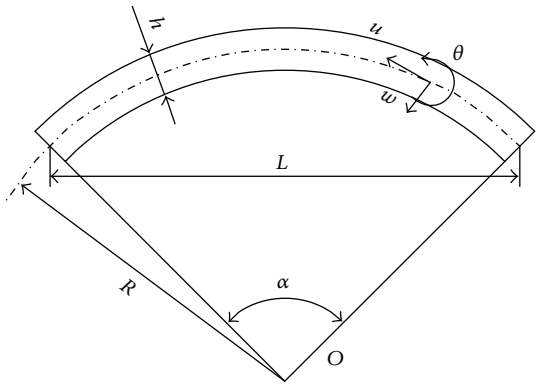

Figure 1: The geometry of curved beam.

Based on their conclusions, a great deal of work was devoted to the development and improvement of curved beam element. Friedman and Kosmatka presented a curved beam element with two nodes and three degrees of freedom per node in [8]; their study took the shear deformable into account. Krishnan and Suresh [9] used a simple cubic linear element to analyze the static and free vibration of arches. By aid of additional internal nodeless degrees of freedom, a higher order hybrid-mixed curved beam element was developed by Kim et al. [10, 11], which enhances the numerical performance of element. In order to improve the element performance, Raveendranath et al. [3, 12] introduced coupled polynomial displacement field into arches analysis. By selecting the trigonometric function as shape function, Leung and Zhu [13] formulated Fourier's element for the analysis of arch vibration. Using the first-order shear deformation theory, Sabir et al. [14] studied the effect of shear deformation on the vibration of circular arches by FEM. And a structural analysis of a curved beam element defined in global coordinates was established by Gimena et al. [15].

The selection of the discrete interpolation function is a key issue in the development of FEM. Wavelet analysis is a new method developed in recent years. In the field of structural analysis, several kinds of wavelet transform functions have been used as interpolation functions to develop wavelet-based finite element formulations for their extraordinary characteristics of integrating the advantages in functional analysis, Fourier's transform, spline analysis, harmonic analysis, and numerical analysis [16–18]. However, most of the wavelet functions used now lack an explicit expression, which would cause trouble and numerical error when finite element solving equation is formulated [19–21]. Compared with the interpolation wavelet function basis used now, B-spline wavelet on the interval (BSWI) basis has the desirable characteristics of compact support, smoothness, and symmetry in addition to the multiresolution analysis [22, 23]. Moreover, it has an explicit expression, which will not lead to any trouble for differentiation and integration. Furthermore, as a type of generalized spline FEM, BSWI element inherits the superiority of spline for structural analysis [24].

Considering the conclusions given by [6, 7], the objective of this study is to present a BSWI (4-order 3-scale) Timoshenko curved beam element for arch analysis. The scaling functions of BSWI wavelets are selected because the scaling functions have excellent analyzing and computing capabilities. The BSWI curved beam element formulation is derived by using the Hamilton principle with the first-order shear deformation theory. The coupling between normal and tangential displacements is considered, and the normal displacement, tangential displacements, and rotation are interpolated by BSWI scaling function, respectively, according to the first-order shear deformation theory. At last, various numerical examples are performed to demonstrate the accuracy and efficiency of the present method with respect to previously published formulations for curved beam.

2. Theoretical Development for Curved Beam

2.1. The Geometry of Curved Beam. The development of a shear deformable curved beam theory is done along the same line as the development for straight beam (Timoshenko beam). The main differences are that the development of the curved beam is performed in a natural coordinate system and there exists a coupling between normal and tangential displacements. These differences make curved beam require three functions (normal, tangential, and rotational) that are coupled in the differential equations rather than two functions (tangential and rotational) for Timoshenko's straight beam. Figure 1 depicts the geometry of a curved beam having a general cross-section of area A and moment of inertia I about the area's centroid and curvature of R. In Figure 1, h indicates the thickness of beam, L is the span of beam, and u, w, and θ present the normal, tangential, and rotational displacements, respectively. We define a natural coordinate system as one in which the x-coordinate is coincident with the centroidal curved axis and y-coordinate is coincident with the principal axes of the cross-section. Similar to Timoshenko's beam, the centroidal axis is the line about which the cross-sections are rotating during bending and therefore represents a zero stress point at each cross-section and is known as the neutral axis. Two parameters are used to depict arches in this study according to the classifications given by [25] the following.

(i) Slenderness ratio (R/h):

(1) thick arch ($R/h < 40$);
(2) moderately thick arch ($R/h = 40$);
(3) thin arch ($R/h > 40$).

(ii) Subtended angle (α (deg.)):

(1) shallow arch ($\alpha < 40$);
(2) moderately deep arch ($\alpha = 40$);
(3) deep arch ($40 < \alpha < 180$);
(4) very deep arches ($\alpha > 180$).

2.2. Energy Functional of Curved Beam. The strain vector $\boldsymbol{\varepsilon} = [\varepsilon_0, \kappa, \gamma_0]^{\mathrm{T}}$ of the curved beam is determined using the definitions for strain in a natural coordinate system, and the nonzero strain components are obtained from the generalized shell theory [10, 11]:

$$\varepsilon_0 = \frac{\partial u}{\partial x} - \frac{v}{R}, \qquad \kappa = \frac{\partial \theta}{\partial x}, \qquad \gamma_0 = \frac{u}{R} + \frac{\partial v}{\partial x} - \theta. \quad (1)$$

For the sake of simplicity, (1) is depicted in the polar coordinate system as

$$\varepsilon_0 = \frac{1}{R}\frac{\partial u}{\partial \alpha} - \frac{v}{R}, \qquad \kappa = \frac{1}{R}\frac{\partial \theta}{\partial \alpha}, \qquad \gamma_0 = \frac{u}{R} + \frac{1}{R}\frac{\partial v}{\partial \alpha} - \theta, \quad (2)$$

where the physical means of α can be found in Figure 1. Using a vector form to rewrite (2), the relations between displacement and strain are

$$\boldsymbol{\varepsilon} = \mathbf{B}_\varepsilon \mathbf{d}, \quad (3)$$

where

$$\mathbf{B}_\varepsilon = \begin{bmatrix} \frac{1}{R}\frac{\partial}{\partial \alpha} & -\frac{1}{R} & 0 \\ 0 & 0 & \frac{1}{R}\frac{\partial}{\partial \alpha} \\ \frac{1}{R} & \frac{1}{R}\frac{\partial}{\partial \alpha} & -1 \end{bmatrix}, \qquad \mathbf{d} = [u, v, \theta]^{\mathrm{T}}. \quad (4)$$

The strain energy is given by

$$U = \frac{1}{2}\int_V \boldsymbol{\varepsilon}^{\mathrm{T}} \mathbf{D} \boldsymbol{\varepsilon}\, \mathrm{d}V. \quad (5)$$

By making use of (3), the strain energy of curved beam is obtained:

$$U = \frac{R}{2}\int_0^{\alpha_E} (\mathbf{B}_\varepsilon \mathbf{d})^{\mathrm{T}} \mathbf{D} \mathbf{B}_\varepsilon \mathbf{d}\, \mathrm{d}\alpha, \quad (6)$$

where $\mathbf{D} = \begin{bmatrix} EA & & \\ & EI & \\ & & kGA \end{bmatrix}$, E and G are Young's and shear moduli, k is the shear modifying factor, and α_E is used to depict ending angle of arch.

Similar to the process of obtaining the strain energy, the kinetic energy of curved beam is obtained by

$$\begin{aligned} T &= \frac{1}{2}\int_V \rho \left[\left(\frac{\partial u}{\partial t}\right)^2 + \left(\frac{\partial v}{\partial t}\right)^2 + \left(\frac{\partial \theta}{\partial t}\right)^2 \right] \mathrm{d}V \\ &= \frac{R}{2}\int_0^{\alpha_E} \frac{\partial \mathbf{d}^{\mathrm{T}}}{\partial t} \begin{bmatrix} \rho A & & \\ & \rho A & \\ & & \rho I \end{bmatrix} \frac{\partial \mathbf{d}}{\partial t} \mathrm{d}\alpha, \end{aligned} \quad (7)$$

where t depicts time and ρ is the mass density of beam material. Also, the work of the external forces is given by

$$W = R\int_0^{\alpha_E} \mathbf{d}^{\mathrm{T}} \mathbf{W}\, \mathrm{d}\alpha, \quad \mathbf{W} = [f \;\; q \;\; m]^{\mathrm{T}}, \quad (8)$$

where f, q, and m are the distributed axial force, radial force, and moment along the length of beam, respectively. By aid of (6)–(8), the total energy of curved beam is formulated as follows:

$$\Pi = U - T - W. \quad (9)$$

Usually, the kinetic energy part is neglected in static analysis, and part of the work from the external forces is neglected when free vibration analysis is needed. Based on (9) and Hamilton's principle, the corresponding terms of BSWI curved beam element static and free vibration analysis are obtained in Section 4.

3. Scaling Functions on the Interval $[0, 1]$

B-spline on interval $[0, 1]$ is given by Quak et al. [26, 27]. Since there should be at least one inner wavelet on the interval $[0, 1]$, the following condition must be satisfied:

$$2^j \geq 2m - 1, \quad (10)$$

where m and j are the order and scale of BSWI, respectively. According to the 0 scale mth order B-spline functions and the corresponding wavelets given by Goswami et al. [27], the j scale mth order BSWI, simply denoted as BSWI m_j, scaling functions $\phi_{m,k}^j(\xi)$ can be evaluated by the following formulas:

$$\phi_{m,k}^j(\xi) = \begin{cases} \phi_{m,k}^l\left(2^{j-l}\xi\right), k = -m+1, \ldots, -1 \\ \quad (0 \text{ boundary scaling functions}) \\ \phi_{m,2^j-m-k}^l\left(1 - 2^{j-l}\xi\right), k = 2^j - m + 1, \ldots, 2^j - 1 \\ \quad (1 \text{ boundary scaling functions}) \\ \phi_{m,0}^l\left(2^{j-l}\xi - 2^{-l}k\right), k = 0, \ldots, 2^j - m \\ \quad (\text{inner scaling functions}). \end{cases} \quad (11)$$

Therefore, the scaling functions on the interval $[0, 1]$ can be written in the vector form as follows:

$$\boldsymbol{\Phi} = \left[\phi_{m,-m+1}^j(\xi) \;\; \phi_{m,-m+2}^j(\xi) \;\; \cdots \;\; \phi_{m,2^j-1}^j(\xi)\right], \quad (12)$$

where ξ belongs to the interval $[0, 1]$. Figure 2 presents the $\mathrm{BSWI4}_3$, which is used in this study as the shape function of curved beam element.

4. Finite Element Formulation Using B-Spline on Interval

Using Hamilton's principle, the following equations of motions can be derived:

$$\delta\Pi = \int_{t_1}^{t_2} (\delta U - \delta T - \delta W)\, \mathrm{d}t = 0. \quad (13a)$$

For static analysis,

$$\delta\Pi = \int_{t_1}^{t_2} (\delta U - \delta W)\, \mathrm{d}t = 0. \quad (13b)$$

For free vibration analysis,

$$\delta\Pi = \int_{t_1}^{t_2} (\delta U - \delta T)\, \mathrm{d}t = 0. \quad (13c)$$

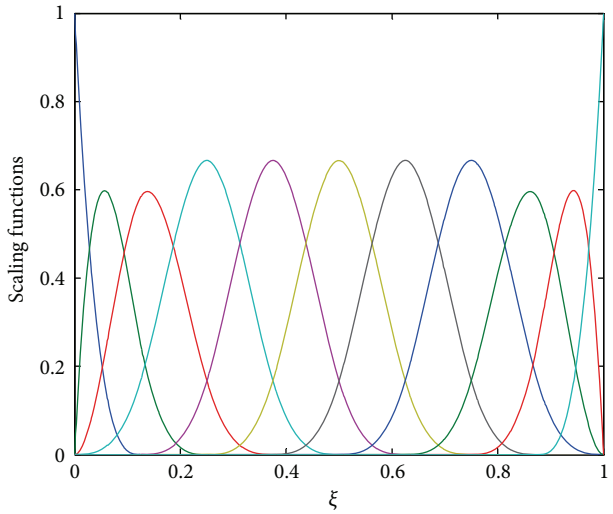

FIGURE 2: BSWI4$_3$ scaling functions on the interval $[0, 1]$.

For the finite element formulation, the normal displacement, tangential displacements, and rotation should be interpolated by BSWI4$_3$ scaling functions, respectively, to follow the first-order shear deformation theory. A displacement field assumption as shown in (14) is made firstly:

$$u = \mathbf{\Phi T u}, \qquad v = \mathbf{\Phi T v}, \qquad \theta = \mathbf{\Phi T \theta}, \tag{14}$$

where $\mathbf{T} = \left[\mathbf{\Phi}^{\mathrm{T}}(\xi_1)\ \ \mathbf{\Phi}^{\mathrm{T}}(\xi_2)\ \cdots\ \mathbf{\Phi}^{\mathrm{T}}(\xi_{n+1})\right]^{-\mathrm{T}}$ is the BSWI element transform matrix. The element displacement field represented by the coefficients of wavelets expansions is transformed from wavelet space to physical space by aid of this transform matrix. In order to give a clear expression, we use some necessary notations here:

$$\begin{aligned}
\boldsymbol{\chi}^{0,0} &= \alpha_E \int_0^1 \mathbf{T}^{\mathrm{T}} \mathbf{\Phi}^{\mathrm{T}} \mathbf{\Phi T}\, \mathrm{d}\xi, \\
\boldsymbol{\chi}^{0,1} &= \int_0^1 \mathbf{T}^{\mathrm{T}} \mathbf{\Phi}^{\mathrm{T}} \frac{\mathrm{d}\mathbf{\Phi}}{\mathrm{d}\xi} \mathbf{T}\, \mathrm{d}\xi, \\
\boldsymbol{\chi}^{1,0} &= \int_0^1 \mathbf{T}^{\mathrm{T}} \frac{\mathrm{d}\mathbf{\Phi}^{\mathrm{T}}}{\mathrm{d}\xi} \mathbf{\Phi T}\, \mathrm{d}\xi, \\
\boldsymbol{\chi}^{1,1} &= \frac{1}{\alpha_E} \int_0^1 \mathbf{T}^{\mathrm{T}} \frac{\mathrm{d}\mathbf{\Phi}^{\mathrm{T}}}{\mathrm{d}\xi} \frac{\mathrm{d}\mathbf{\Phi}}{\mathrm{d}\xi} \mathbf{T}\, \mathrm{d}\xi, \\
\boldsymbol{\chi}^{1,2} &= \frac{1}{\alpha_E^2} \int_0^1 \mathbf{T}^{\mathrm{T}} \frac{\mathrm{d}\mathbf{\Phi}^{\mathrm{T}}}{\mathrm{d}\xi} \frac{\mathrm{d}^2\mathbf{\Phi}}{\mathrm{d}\xi^2} \mathbf{T}\, \mathrm{d}\xi, \\
\boldsymbol{\chi}^{2,1} &= \frac{1}{\alpha_E^2} \int_0^1 \mathbf{T}^{\mathrm{T}} \frac{\mathrm{d}^2\mathbf{\Phi}^{\mathrm{T}}}{\mathrm{d}\xi^2} \frac{\mathrm{d}\mathbf{\Phi}}{\mathrm{d}\xi} \mathbf{T}\, \mathrm{d}\xi, \\
\boldsymbol{\chi}^{2,2} &= \frac{1}{\alpha_E^3} \int_0^1 \mathbf{T}^{\mathrm{T}} \frac{\mathrm{d}^2\mathbf{\Phi}^{\mathrm{T}}}{\mathrm{d}\xi^2} \frac{\mathrm{d}^2\mathbf{\Phi}}{\mathrm{d}\xi^2} \mathbf{T}\, \mathrm{d}\xi.
\end{aligned} \tag{15}$$

Substituting (14) with (13b), a finite element formulation of curved beam static analysis can be obtained:

$$\begin{aligned}
\mathbf{K\Delta} &= \mathbf{P}, \\
\mathbf{K} &= \frac{1}{R} \int_0^{\alpha_E} \mathbf{B}_\varepsilon^{\mathrm{T}} \mathbf{D} \mathbf{B}_\varepsilon \mathrm{d}\alpha, \\
\mathbf{P} &= R \int_0^{\alpha_E} (\mathbf{\Phi T})^{\mathrm{T}} \begin{bmatrix} f & & \\ & q & \\ & & m \end{bmatrix} \mathrm{d}\alpha,
\end{aligned} \tag{16}$$

where $\mathbf{\Delta} = \left[\mathbf{u}\ \ \mathbf{v}\ \ \boldsymbol{\theta}\right]^{\mathrm{T}}$ is the vector formulation of element displacement, $\mathbf{K}$ is the stiffness matrix, and $\mathbf{P}$ is the force vector. The details of the stiffness matrix are

$$\mathbf{K} = \frac{1}{R} \times \begin{bmatrix} EA\boldsymbol{\chi}^{1,1} + kGA\boldsymbol{\chi}^{0,0} & -EA\boldsymbol{\chi}^{1,0} + kGA\boldsymbol{\chi}^{0,1} & -RkGA\boldsymbol{\chi}^{0,0} \\ -EA\boldsymbol{\chi}^{0,1} + kGA\boldsymbol{\chi}^{1,0} & EA\boldsymbol{\chi}^{0,0} + kGA\boldsymbol{\chi}^{1,1} & -RkGA\boldsymbol{\chi}^{1,0} \\ -RkGA\boldsymbol{\chi}^{0,0} & -RkGA\boldsymbol{\chi}^{0,1} & EI\boldsymbol{\chi}^{1,1} + R^2 kGA\boldsymbol{\chi}^{0,0} \end{bmatrix}. \tag{17}$$

Substituting (14) with (13c), a finite element formulation of arch free vibration analysis is obtained as a generalized eigenproblem:

$$\left(\mathbf{K} - \omega^2 \mathbf{M}\right) \mathbf{X} = 0, \tag{18}$$

where ω is the natural frequency and $\mathbf{X}$ is the mode shape of arches. The mass matrix $\mathbf{M}$ is defined as

$$\mathbf{M} = R \int_0^{\alpha_E} (\mathbf{\Phi T})^{\mathrm{T}} \begin{bmatrix} \rho A & & \\ & \rho A & \\ & & \rho I \end{bmatrix} \mathbf{\Phi T}\, \mathrm{d}\alpha. \tag{19}$$

5. Numerical Examples

The validity and efficiency of the element formulated in the previous section are verified through numerical examples in this part, and static and dynamic numerical examples are given, respectively.

5.1. Static Analysis

5.1.1. A Quarter Circular Cantilever Arch. The model consists of a quarter circular cantilever arch, where the origin of coordinate is at the fixed end, as shown in Figure 3. The quarter ring is subjected to a radial tip load. This moderately deep arch is idealized with one BSWI element and analyzed for a wide range of thick to thin beams by changing the slenderness ratio of R/h. The exact solution for this problem is derived using Castigliano's energy theorem as [28]

$$u_{\mathrm{C}} = \frac{PR^3}{2EI} - \frac{PR}{2kGA} - \frac{PR}{2EA}, \tag{20a}$$

$$v_{\mathrm{C}} = \frac{\pi PR^3}{4EI} + \frac{\pi PR}{4kGA} + \frac{\pi PR}{4EA}, \tag{20b}$$

$$\theta_{\mathrm{C}} = \frac{PR^2}{EI}. \tag{20c}$$

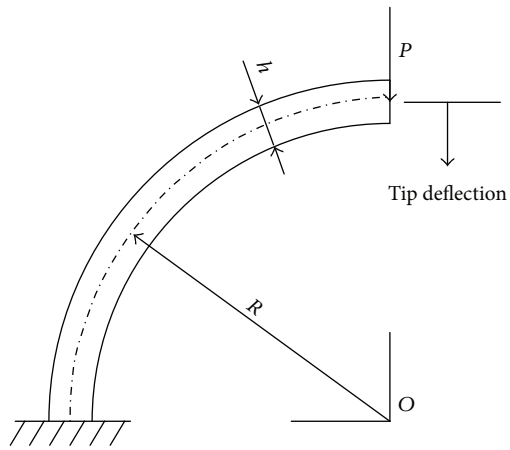

Figure 3: Geometry and loading of a circular cantilever arch.

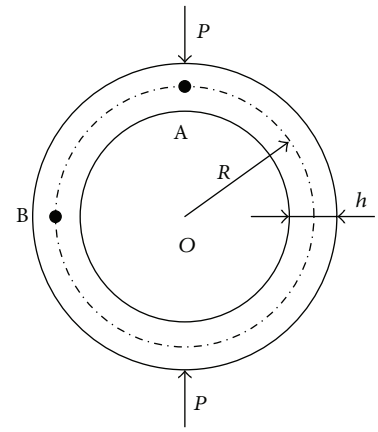

Figure 4: Geometry and loading of a pinched ring.

In Table 1, MFE method [3] and the solution given by Lee and Sin [28] are used to contrast with the present method. In order to compare them with the exact solutions given by (20a)–(20c), we transform the data into the form of a ratio between numerical result and exact solution. It is noteworthy that the presence of BSWI is analogous to MFE, and the accuracy of v and θ is better than MFE in a wide range of thick to thin beams, even in the thick condition. Compared with the solution given by [28], the present method also shows its superiority.

5.1.2. A Pinched Ring. Babu and Prathap [29] considered that the pinched ring is the best example to demonstrate the behavior of the elements in a deep arch configuration. Figure 4 depicts a pinched ring, on which the same radial loads are applied at the top and bottom of the ring. The physical model is idealized with one BSWI element and analyzed for a wide range of thick to thin beams by changing the slenderness ratio of R/h. The exact solution of points A and B is derived by means of Castigliano's energy theorem as [28]

$$v_{AC} = \frac{PR^3}{EI}\frac{\pi^2 - 8}{4\pi} + \frac{\pi PR}{4kGA} + \frac{\pi PR}{4EA}, \tag{21}$$

$$v_{BC} = -\left(\frac{PR^3}{EI}\frac{4 - \pi}{2\pi} + \frac{PR}{2kGA} - \frac{PR}{2EA}\right). \tag{22}$$

Numerical results calculated by BSWI are shown in Table 2, and, as a reference, the solution given by Lee and Sin [28] is also shown there. It can be seen that the present method has a satisfying accuracy in a wide range of slenderness ratio. Although there are some slight accuracy losses with tangential displacement of point B when slenderness ratio is big, it is still in an acceptable confine. It should be noticed that the present method shows a good presence for the calculation of tangential displacement of point A.

5.1.3. A Nearly Straight Cantilever Curved Beam. In order to validate the reducibility of the present curved beam element to straight beam configuration, a numerical example as shown in Figure 5 is given. This arch has a very large radius and short span subjected to a concentrated load. The properties are $R = 2000$ m, $L = 100$ m, $h = 10$ m, $P = 1$ N, $E = 1 \times 10^6$ Pa, Poisson's ratio $\mu = 0.3$, and width of beam $b = 30$ m. It should be mentioned that the properties presented above are defined in SI (System International), but all closed-form unit systems are suitable in this example; they will not influence the solved values. This structure is modeled using one BSWI element. For this type of thin beam ($R/h > 40$), the exact solutions of tip displacement v for the three kinds of load conditions shown in Figure 5 are given by [3]

$$v_a = \frac{PL^3}{3EI}\left(1 + \frac{6I(1+\mu)}{kL^2A}\right), \tag{23}$$

$$v_b = \frac{qL^4}{8EI}\left(1 + \frac{8I(1+\mu)}{kL^2A}\right), \tag{24}$$

$$v_c = \frac{qL^4}{30EI}\left(1 + \frac{10I(1+\mu)}{kL^2A}\right). \tag{25}$$

Equations (23)–(25) correspond to Figures 5(a)–5(c), respectively. Table 3 presents the comparison of numerical results and the exact solution in which the relative errors are all less than 1%. Thus, the present method has a good reducibility to straight beam configuration.

5.2. Free Vibration Analysis

5.2.1. A Hinged Arch. Figure 6 gives the geometry of a hinged arch which is widely analyzed in previously published works. The following properties of arch are employed for the computation: $R = 12$ in, $h = 0.25$ in, $A = 0.1563$ in^2, $I = 8.138 \times 10^{-4}$ in^4, $k = 0.8497$, $E = 3.04 \times 10^7$ psi, $\mu = 0.3$, and $\rho = 0.02763$ slugs ft/in^4.

In order to test the accuracy of the present method for the change of subtended angle, the whole results for shallow arch, moderately deep arch, deep arch, and very deep arches, as classified in [25], are given in Table 4. With a various subtended angle α ranging from 10 to 350 degrees, Table 4 shows the comparisons of fundamental natural frequency

Table 1: Comparisons of the present solutions of the one quarter ring with Castigliano's energy solution and other methods.

Slenderness ratio (R/h)	MFE [3]			Lee and Sin [28]			Present		
	u/u_C	v/v_C	θ/θ_C	u/u_C	v/v_C	θ/θ_C	u/u_C	v/v_C	θ/θ_C
5	1.0124	0.9996	0.9997	0.99916	1.01494	1.00000	1.0129	1.0000	1.0000
10	1.0036	1.0000	0.9999	0.99968	1.00354	1.00000	1.0052	1.0000	1.0000
20	1.0010	1.0000	1.0000	0.99981	1.00072	1.00000	1.0013	1.0000	1.0000
100	1.0001	1.0000	0.9997	0.99986	0.99982	1.00000	1.0000	1.0000	1.0000
200	1.0001	1.0000	0.9999	0.99986	0.99979	1.00000	1.0000	0.9999	1.0000
1000	1.0001	1.0000	0.9999	0.99986	0.99978	1.00000	0.9999	0.9998	0.9995

Table 2: Comparisons of the present solutions of the pinched ring with Castigliano's energy solution and the solution given by [28].

Slenderness ratio (R/h)	Lee and Sin [28]		Present	
	v_A/v_{AC}	v_B/v_{BC}	v_A/v_{AC}	v_B/v_{BC}
2.5	0.98730	0.98533	1.00000	1.08543
5	0.99574	0.99556	1.00000	1.03484
10	0.99834	0.99828	1.00000	1.00869
20	0.99904	0.99897	1.00000	1.00209
100	0.99923	0.99918	0.99998	1.00005
200	0.99927	0.99924	0.99991	0.99988
1000	0.99925	0.99922	0.99777	0.99662

Table 3: Numerical results for the tip displacement (m) of a nearly straight cantilever curved beam.

Load	Present ($\times 10^{-5}$)	Exact solution ($\times 10^{-5}$)	Relative error
Concentrated	1.338	1.344	0.44%
Uniform distributed	50.255	50.520	0.53%
Linear distributed	13.419	13.507	0.65%

(rad/s) of the hinged arch. The present solution is computed by four BSWI elements. Compared with the solutions given by CHM2 [11], THICK-2 [13], MFE [30], and E1.1b [31], the present element shows good consistency with them. In order to represent this clearly, Figure 7 is presented. In Figure 7, numerical results are normalized by those obtained by THICK-2, which could be seen as a relative accurate solution. It is clear that the present solution is bounded by E1.1b and CHM2. Specifically, the current solution has a good agreement with the solution given by THICK-2. Thus the accuracy of the present method is validated.

5.2.2. A Thin Circular Ring. The geometry of a circular ring has been given in Figure 4. Different from the problem considered for a pinched ring mentioned above, there exists no external force for the free vibration of circular ring. Timoshenko [32] gave the exact solution of the ith order natural vibration of a thin ring:

$$\omega_i = \sqrt{\frac{EIi^2\left(1-i^2\right)^2}{\rho AR^4\left(1+i^2\right)}}. \tag{26}$$

Considering the classifications given by [25], we use the slenderness ratio $R/h > 40$ to depict thin rings. Thus the slenderness ratio ranging from 50 to 1000 is studied in Table 5. The other properties for the model are $R = 0.3048$ m, $E = 1.31 \times 10^{11}$ Pa, $\mu = 0.3$, and $\rho = 1741$ kg/m^3. Two BSWI elements are used to idealize the model. Table 5 presents the first four order mode frequencies for ring, including the rigid body mode. The numerical results obtained using BSWI agree well with the exact solutions.

5.2.3. A 90° Arch with Different Boundaries. In this example, free vibrations of a 90° arch with different boundaries are analyzed to test the adaptability of BSWI element. The dimensionless frequency of the arch is defined as $C_i = \omega_i \alpha^2 R^2 \sqrt{\rho A/EI}$. The main property of arch is R/r, where r is the radius of gyration $\sqrt{I/A}$. Arches ($R/r = 100$) with different boundaries are studied, and the numerical results are presented in Table 6. The results show that the present method has a good agreement with the references.

5.2.4. A Three-Span Clamped Arch. This example is a curved beam with three subspans of equal span angle and different radiuses of curvature are depicted in Figure 8. The total span angle is 180° and each subspan angle is 60°. In this example, three BSWI elements are used to idealize this model. In contrast, the dimensionless frequency of the arch ($R/r = 100$) is selected as $C_i = \omega_i R^2 \sqrt{\rho A/EI}$, which is slightly different from the C_i used in Section 5.2.3. The problem presented here has also been solved by applying the finite element method (FEM) [9, 33] and the wave analysis method [34]. In Table 7, the dimensionless frequencies obtained from the present approach are compared with those of [9, 33, 34]. It is noticed that the natural frequencies obtained from the BSWI agree well with these solutions, especially with [34], which

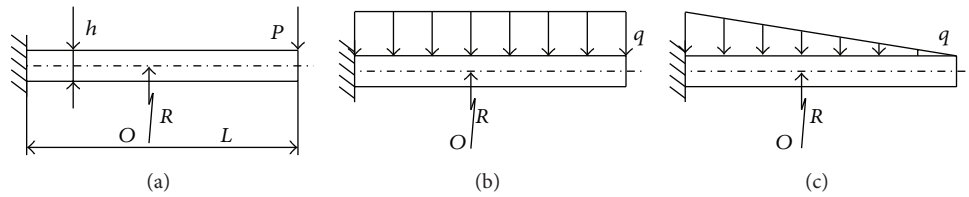

Figure 5: Geometry and loading of a nearly straight cantilever curved beam: (a) concentrated load, (b) uniform distributed load, and (c) linear distributed load.

Table 4: Fundamental frequency (rad/s) of a hinged arch with various subtended angles.

Angles (deg.)	CHM2 [11]	THICK-2 [13]	MFE [30]	E1.1b [31]	Present
10	5845.78	5841.74	5852.32	5874.30	5881.64
20	2836.20	2827.63	2829.66	2823.10	2829.13
30	2370.01	2339.82	2373.23	2345.20	2348.11
60	564.05	560.25	567.71	561.20	560.62
90	230.31	229.66	232.94	230.40	229.69
120	115.82	115.64	117.50	116.30	115.64
150	64.52	64.43	76.24	64.93	64.42
180	37.91	37.86	38.71	38.24	37.85
210	22.80	22.77	23.42	23.05	22.76
240	13.69	13.66	14.19	13.87	13.66
270	7.94	7.92	8.39	8.06	7.92
300	4.20	4.18	4.65	4.27	4.19
330	1.70	1.69	2.28	1.73	1.69
350	0.50	0.49	1.38	0.50	0.50

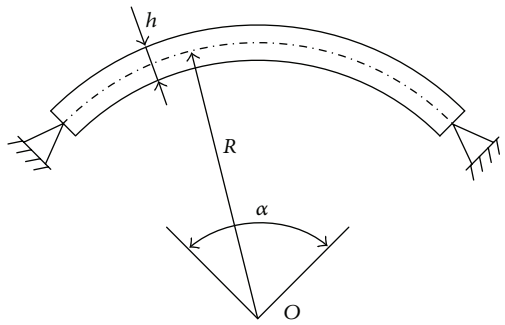

Figure 6: Geometry of a hinged arch.

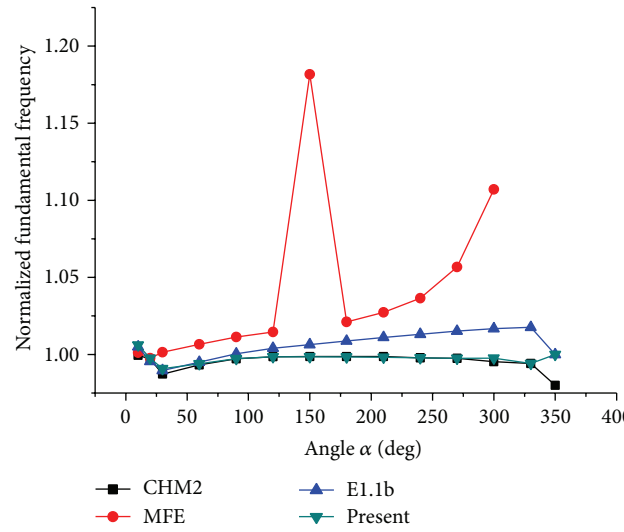

Figure 7: Normalized fundamental frequency for a hinged arch.

can be seen as a relative accurate reference solution for this problem [34].

6. Conclusions

A B-spline wavelet on interval curved beam element is constructed in this paper. This method gives satisfactory results for static and free vibration behaviors of arches with varied curvatures, thicknesses, and boundaries. The reason for getting acceptable results can be attributed to the fact that the present element is developed in generalized shell theory, which is adapted to obtain the couple of normal, tangential, and rotational displacement. Another reason for getting acceptable results can be attributed to the numerical properties of B-spline wavelet on interval. By means of the numerical examples, the accuracy and efficiency of the present element are validated. It can be seen that the proposed method can obtain good results for static and free vibration analysis. The methodology and results presented here can help in understanding the more complicated behavior of the curved shell element.

Table 5: Frequencies (rad/s) of a thin circular ring with various slenderness ratios.

Slenderness ratio (R/h)	Method	Mode			
		Rigid body	1	2	3
50	Present	0.021	70.158	198.397	380.314
	Timoshenko [32]	0	70.169	198.469	380.546
100	Present	0.021	35.085	99.237	190.301
	Timoshenko [32]	0	35.085	99.234	190.273
200	Present	0.021	17.545	49.640	95.240
	Timoshenko [32]	0	17.542	49.617	95.137
500	Present	0.020	7.023	19.899	38.229
	Timoshenko [32]	0	7.017	19.847	38.055
800	Present	0.020	4.394	12.474	23.968
	Timoshenko [32]	0	4.386	12.404	23.784
1000	Present	0.019	3.518	10.002	19.212
	Timoshenko [32]	0	3.508	9.923	19.027

Table 6: First and second lowest dimensionless frequencies of 90° arch with different boundaries.

Boundary condition	Method	Mode	
		1	2
Hinged-hinged	Raveendranath et al. [3]	33.83	78.72
	Krishnan and Suresh [9]	33.93	79.42
	Sabir et al. [14]	33.79	79.02
	Present	33.87	78.95
Clamped-clamped	Raveendranath et al. [3]	55.34	102.28
	Krishnan and Suresh [9]	55.82	104.28
	Sabir et al. [14]	55.45	103.59
	Present	55.54	103.00
Clamped-hinged	Raveendranath et al. [3]	43.81	90.60
	Krishnan and Suresh [9]	44.05	91.82
	Sabir et al. [14]	43.81	91.29
	Present	43.91	91.00

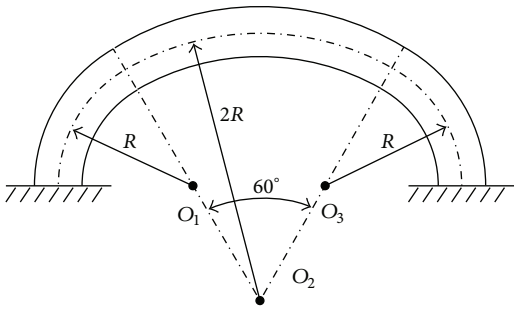

Figure 8: Geometry of a three-span clamped arch.

Conflict of Interests

The authors declare that there is no conflict of interests regarding the publication of this paper.

Table 7: Dimensionless frequencies of the three-span clamped arch.

Mode	Krishnan and Suresh [9]	Maurizi et al. [33]	Kang et al. [34]	Present
1	2.701	2.680	2.6833155	2.682
2	4.828	4.824	4.8337572	4.828
3	9.543	9.536	9.5647244	9.549
4	14.535	14.527	14.5850042	14.551
5	21.751	21.749	21.8646005	21.795

Acknowledgments

Special thanks should be expressed to the editor and anonymous referees for their constructive suggestions as well as the patience and efforts they paid in the language correction of the paper. This work was supported by the National Natural Science Foundation of China (nos. 51225501 and 51075314) and the Program for Changjiang Scholars and Innovative Research Team in University.

References

[1] D. L. Thomas, J. M. Wilson, and R. R. Wilson, "Timoshenko beam finite elements," *Journal of Sound and Vibration*, vol. 31, no. 3, pp. 315–330, 1973.

[2] A. P. Boresi and O. M. Sidebottom, *Advanced Mechanics of Materials*, John Wiley & Sons, Hoboken, NJ, USA, 1985.

[3] P. Raveendranath, G. Singh, and G. V. Rao, "A three-noded shear-flexible curved beam element based on coupled displacement field interpolations," *International Journal for Numerical Methods in Engineering*, vol. 51, no. 1, pp. 85–101, 2001.

[4] G. Cantin and R. W. Clough, "A curved, cylindrical-shell, finite element," *American Institute of Aeronautics and Astronautics Journal*, vol. 6, no. 6, pp. 1057–1062, 1968.

[5] D. Ashwell and A. Sabir, "A new cylindrical shell finite element based on simple independent strain functions," *International Journal of Mechanical Sciences*, vol. 14, no. 3, pp. 171–183, 1972.

[6] H. Meck, "An accurate polynomial displacement function for unite ring elements," *Computers & Structures*, vol. 11, no. 4, pp. 265–269, 1980.

[7] Y. Yamamoto and H. Ohtsubo, "A qualitative accuracy consideration on arch elements," *International Journal for Numerical Methods in Engineering*, vol. 18, no. 8, pp. 1179–1195, 1982.

[8] Z. Friedman and J. Kosmatka, "An accurate two-node finite element for shear deformable curved beams," *International Journal for Numerical Methods in Engineering*, vol. 41, no. 3, pp. 473–498, 1998.

[9] A. Krishnan and Y. Suresh, "A simple cubic linear element for static and free vibration analyses of curved beams," *Computers & Structures*, vol. 68, no. 5, pp. 473–489, 1998.

[10] J. G. Kim and Y. Y. Kim, "A new higher-order hybrid-mixed curved beam element," *International Journal for Numerical Methods in Engineering*, vol. 43, no. 5, pp. 925–940, 1998.

[11] J.-G. Kim and Y.-K. Park, "Hybrid-mixed curved beam elements with increased degress of freedom for static and vibration analyses," *International Journal for Numerical Methods in Engineering*, vol. 68, no. 6, pp. 690–706, 2006.

[12] P. Raveendranath, G. Singh, and B. Pradhan, "Free vibration of arches using a curved beam element based on a coupled polynomial displacement field," *Computers & Structures*, vol. 78, no. 4, pp. 583–590, 2000.

[13] A. Y. T. Leung and B. Zhu, "Fourier p-elements for curved beam vibrations," *Thin-Walled Structures*, vol. 42, no. 1, pp. 39–57, 2004.

[14] A. Sabir, M. Djoudi, and A. Sfendji, "The effect of shear deformation on the vibration of circular arches by the finite element method," *Thin-Walled Structures*, vol. 18, no. 1, pp. 47–66, 1994.

[15] L. Gimena, F. Gimena, and P. Gonzaga, "Structural analysis of a curved beam element defined in global coordinates," *Engineering Structures*, vol. 30, no. 11, pp. 3355–3364, 2008.

[16] L. A. Díaz, M. T. Martín, and V. Vampa, "Daubechies wavelet beam and plate finite elements," *Finite Elements in Analysis and Design*, vol. 45, no. 3, pp. 200–209, 2009.

[17] Y. T. Zhong and J. W. Xiang, "Construction of wavelet-based elements for static and stability analysis of elastic problems," *Acta Mechanica Solida Sinica*, vol. 24, no. 4, pp. 355–364, 2011.

[18] Z. Yang, X. F. Chen, B. Li, Z. J. He, and H. H. Miao, "Vibration analysis of curved shell using B-spline wavelet on the interval (BSWI) finite elements method and general shell theory," *Computer Modeling in Engineering & Sciences*, vol. 85, no. 2, pp. 129–156, 2012.

[19] W.-Y. He and W.-X. Ren, "Finite element analysis of beam structures based on trigonometric wavelet," *Finite Elements in Analysis and Design*, vol. 51, pp. 59–66, 2012.

[20] J.-G. Han, W.-X. Ren, and Y. Huang, "A spline wavelet finite element formulation of thin plate bending," *Engineering with Computers*, vol. 25, no. 4, pp. 319–326, 2009.

[21] Z. Yang, X. Chen, X. Zhang, and Z. He, "Free vibration and buckling analysis of plates using B-spline wavelet on the interval Mindlin element," *Applied Mathematical Modelling*, vol. 37, no. 5, pp. 3449–3466, 2012.

[22] J. Xiang, J. Long, and Z. Jiang, "A numerical study using Hermitian cubic spline wavelets for the analysis of shafts," *Proceedings of the Institution of Mechanical Engineers C*, vol. 224, no. 9, pp. 1843–1851, 2010.

[23] J. Xiang, T. Matsumoto, Y. Wang, and Z. Jiang, "A hybrid of interval wavelets and wavelet finite element model for damage detection in structures," *Computer Modeling in Engineering & Sciences*, vol. 81, no. 3-4, pp. 269–294, 2011.

[24] J. W. Xiang and M. Liang, "Multiple damage detection method for beams based on multi-scale elements using hermite cubic splinewavelet," *Computer Modeling in Engineering & Sciences*, vol. 73, no. 3, pp. 267–298, 2011.

[25] R. H. Gallagher, *Finite Elements for Thin Shells and Curved Members*, John Wiley & Sons, New York, NY, USA, 1976.

[26] E. Quak and N. Weyrich, "Decomposition and reconstruction algorithms for spline wavelets on a bounded interval," *Applied and Computational Harmonic Analysis*, vol. 1, no. 3, pp. 217–231, 1994.

[27] J. C. Goswami, A. K. Chan, and C. K. Chui, "On solving first-kind integral equations using wavelets on a bounded interval," *IEEE Transactions on Antennas and Propagation*, vol. 43, no. 6, pp. 614–622, 1995.

[28] P.-G. Lee and H.-C. Sin, "Locking-free curved beam element based on curvature," *International Journal for Numerical Methods in Engineering*, vol. 37, no. 6, pp. 989–1007, 1994.

[29] C. R. Babu and G. Prathap, "A linear thick curved beam element," *International Journal for Numerical Methods in Engineering*, vol. 23, no. 7, pp. 1313–1328, 1986.

[30] P. Raveendranath, G. Singh, and B. Pradhan, "A two-noded locking–free shear flexible curved beam element," *International Journal for Numerical Methods in Engineering*, vol. 44, no. 2, pp. 265–280, 1999.

[31] A. Krishnan, S. Dharmaraj, and Y. Suresh, "Free vibration studies of arches," *Journal of Sound and Vibration*, vol. 186, no. 5, pp. 856–863, 1995.

[32] S. Timoshenko, *Vibration Problems in Engineering*, John Wiley & Sons, Hoboken, NJ, USA, 1974.

[33] M. Maurizi, P. M. Belles, R. E. Rossi, and M. A. de Rosa, "Free vibration of a three-centered arc clamped at the ends," *Journal of Sound and Vibration*, vol. 161, no. 1, pp. 187–189, 1993.

[34] B. Kang, C. Riedel, and C. Tan, "Free vibration analysis of planar curved beams by wave propagation," *Journal of Sound and Vibration*, vol. 260, no. 1, pp. 19–44, 2003.